THE JOURNAL OF PHYSICAL CHEMISTRY A

Article

Cite This: J. Phys. Chem. A XXXX, XXX, XXX−XXX

pubs.acs.org/JPCA

Studies of Arabinose- and Mannose-Related Anionic Species and Comparison to Ribose and Fructose

Zhen Zeng and Elliot R. Bernstein*

Department of Chemistry, NSF ERC for Extreme Ultraviolet Science and Technology, Colorado State University, Fort Collins, Colorado 80523, United States

Supporting Information

ABSTRACT: Gas phase, isolated monosaccharides arabinose- and mannose-related anionic species generated through the matrix-assisted laser desorption ionization (MALDI) method are investigated via negative ion photoelectron spectroscopy (PES) and density functional theory (DFT) calculations. The vertical detachment energies (VDEs) of the observed anionic species are experimentally determined: the corresponding structures are assigned based on good agreement between experimental and theoretical VDEs. Arabinose$^-$ parent anion is found to exist as open chain structures in the gas phase, while mannose$^-$ parent anionic species are not observed. Both monosaccharides undergo dissociation through loss of H and loss of H_2O. (saccharide-H)$^-$ anions evidence coexisting positional and conformational isomers. (saccharide-H_2O)$^-$ species have only two positional isomers, each with conformational differences. The present results for arabinose and mannose are further compared to those previously reported for ribose and fructose. This comparison is based on the anions observed and identified through the same PES/DFT techniques for the four saccharides (arabinose, mannose, ribose, and fructose). The issue of natural selection of ribose as the sugar backbone constituent of RNA is thereby explored from the point of view of anionic electronic structure and stability of the four species. Saccharide phosphates are also discussed in the present work with regard to addressing the unique natural selection of ribose for the backbone support of RNA and DNA.

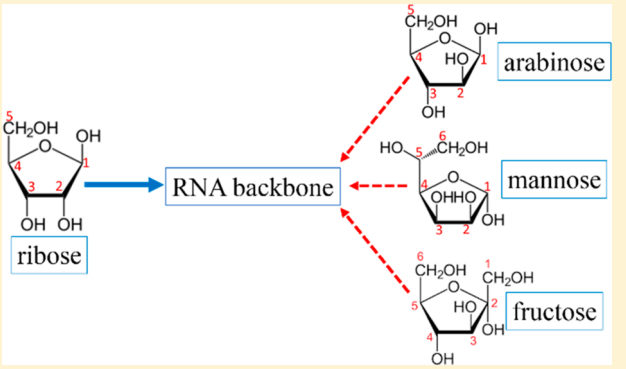

I. INTRODUCTION

Arabinose and mannose, two biologically important monosaccharides, are considered in this report with regard to their neutral and anionic species behaviors. These properties are further compared to those found for similar saccharides fructose[1] and ribose.[2] All four molecular and anionic forms are compared, contrasted, and analyzed with regard to their usefulness toward stabilizing RNA and DNA in a reducing, high intensity ultraviolet radiation (UV), and electron rich environment. L-arabinose, as a naturally occurring aldopentose and plant saccharide, is widely found as a component of biopolymers (such as, hemicellulose and pectin) in plant cell walls.[3−6] Arabinose predominantly exists as a pyranose in solution and the solid-state. Aldohexose mannose plays an essential and important role in the human metabolism system, such as *N*-linked glycosylation of proteins.[7,8] The anomeric form of mannose is present as α- and β-pyranose with a natural proportion of 67:33 in aqueous solution.[9]

To the best of our knowledge, structural and electronic investigations have not been conducted for isolated, anionic mannose and arabinose. The anionic state of monosaccharides is important for understanding the corresponding stability and fragmentation mechanisms of their respective parent neutral forms. In this context, a systematic study of the parent species, as well as their dissociation-related gas phase ions, is essential.

Exclusive natural selection of the monosaccharide ribose for the saccharide backbone subunit of DNA/RNA has been a central concern for the field of prebiotic chemistry. The ribonucleotides have nine required chemoselectivities,[10] such as aldopentose and ribo in the furanosyl form, as presented in some detail in ref 10. Selection criteria for the evolutionary choice of ribose over other saccharides have been suggested to be associate with size, steric effects, rigidity of nucleotide, chemical stability,[11−14] enantiomeric purity,[15] and nucleoside formation activation.[16]

Secondary low energy electron radiation has been considered to induce DNA damage (single- and/or double-strand breaks).[17,18] The formation of transient anions is suggested to play an essential role in the fragmentation of DNA associated with low electron energy.[19] The sugar moiety of thymidine can capture a low energy electron and undergo N1−C1 bond rupture through dissociative electron attachment.[20] The overall comparison between different mono-

Received: December 8, 2018
Revised: January 30, 2019
Published: February 26, 2019

DOI: 10.1021/acs.jpca.8b11838
J. Phys. Chem. A XXXX, XXX, XXX−XXX

saccharides (here ribose, mannose, arabinose, fructose) in their various anionic forms is essential for the understanding of RNA/DNA stability toward damage due to low energy electrons, ionizing radiation, and/or acid/base conditions (e^-/VUV/pH), such as proposed for the prebiotic, reducing environment of early Earth.

In the present work, we combine PES experiments and DFT calculations to investigate the electronic and geometric structures of gas phase, isolated arabinose and mannose (Figure 1) related anionic species generated through the

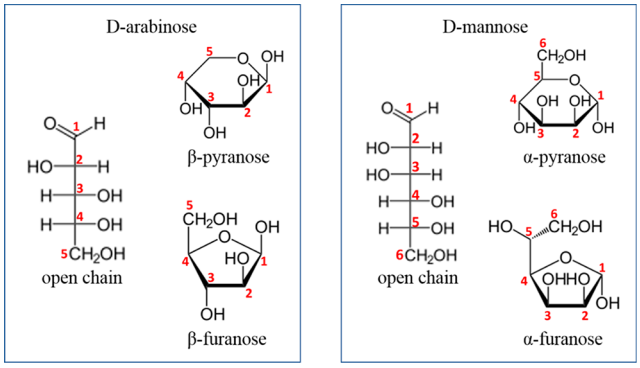

Figure 1. Schematic structures of D-arabinose (left) and D-mannose (right).

matrix-assisted laser desorption/ionization (MALDI) method. The arabinose$^-$ parent anion is detected in these experiments, but the mannose$^-$ parent anion is not. Fragmentation ions (arabinose-H)$^-$, (arabinose-H_2O)$^-$, (mannose-H)$^-$, and (mannose-H_2O)$^-$ are additionally observed: their anionic structures in the present experiments are definitively assigned based on the agreement between calculated and observed VDEs. A comparison between the four monosaccharide (arabinose, mannose, ribose, fructose) results is discussed in detailed in the terms of the corresponding observed and calculated anionic form behaviors. Saccharide phosphates, an integral part of the structural framework of DNA/RNA, have also been taken into consideration for the natural selection issues. D-Ribose-5-phosphate and D-fructose-6-phosphate are chosen, and their anionic species and accompanying dissociation related anions are analyzed in this regard.

II. EXPERIMENTAL PROCEDURES

The experimental apparatus consists of three parts: a pulsed supersonic nozzle with an attached matrix-assisted laser desorption ionization (MALDI) source, a reflectron time-of-flight mass spectrometer (RTOFMS), and a magnetic bottle photoelectron TOF spectrometer (MBTOFPES). Details of this system (RTOFMS/MBTOFPES) can be found in our previous publications.[21,22] The nozzle employed for the sample beam generation is constructed from a Jordan Co. pulsed valve and a laser desorption attachment. All sample drums for MALDI are prepared by wrapping a Zn substrate on a clean Al drum.[23] A mixed solution of D-arabinose or D-mannose and matrix (R6G or DCM) dye with mole ratio ~3:2 in a solvent (typically, methanol or acetonitrile) is uniformly sprayed on the drum/substrate surface using an air atomizing spray nozzle (Spraying System Co.) with siphon pressure of 10 psig. For saccharide phosphate experiments, the D-ribose 5-phosphate salt or D-fructose 6-phosphate salt sample is dissolved in a solution with pH of ~5. During the spraying process, the sample drum is rotated under heat of a halogen lamp in a fume hood to ensure that deposition of sample and matrix on the drum surface is homogeneous and dry. The well-coated and dried sample drum is then placed in the laser ablation head/nozzle assembly and put into the vacuum chamber. Second harmonic (532 nm) light pulses from a Nd:YAG laser are used to ablate the sample drum, which rotates and translates simultaneously to maintain a fresh sample area for each laser ablation pulse. Intact D-arabinose or D-mannose molecules are desorbed from the drum, interact with other species (including electrons) in the ablated material plume, are entrained in the supersonic flow of helium carrier gas with a 50 psi backing pressure through a 2 × 60 mm channel in the ablation head, and expanded into the sample chamber. With a closed pulsed valve, the RTOFMS chamber pressure is ~6×10^{-8} Torr. Generated molecular anions are pulsed into the RTOFMS and are mass analyzed using the RTOFMS. For PES experiments, specific anions are first mass selected and decelerated before interacting with a 355 nm (3.496 eV), or 266 nm (4.661 eV) laser beam from another Nd:YAG laser in the photodetachment region. Photodetached electrons are collected and energy analyzed by the MBTOFPES at nearly 100% efficiency. The photodetachment laser is operated at a 10 Hz repetition rate, while the ablation laser is synchronously triggered at 5 Hz. Data are collected at 5 Hz employing a background subtraction with alternation of the ablation laser on/off if the detachment laser generates 266 nm or higher energy photons. Every photoelectron spectrum is calibrated by the known spectra of Cu^- at the employed detachment photon energy. The photoelectron energy resolution is ~4% (40 meV for 1 eV kinetic energy electrons), as anticipated for a 1 m PES flight tube.

III. COMPUTATIONAL METHODS

In the present work, all calculations are executed using density function theory (DFT) employing Becke's three-parameter hybrid (B3LYP)[24−26] functional and a 6-311++G(d,p) basis set for all atoms, as implemented in the Gaussian 09 program.[27] The B3LYP/6-311++G(d,p) level of theory has been validated to be efficient and accurate for electronic and geometric property calculations of gas phase sugar molecular anions and neutrals based on previous studies.[1,2] No symmetry restrictions are applied for the calculations. Optimization of the low-lying isomers for each anion are performed with harmonic vibrational frequencies calculated to confirm that the obtained structures are the true local minima. Theoretical VDEs for each anionic species are calculated as the energy difference between the ground state of the anion and its corresponding neutral at the same structure as the anion. For further electronic structure based understanding of the observed arabinose and mannose parent anionic species behavior, a natural bond orbital (NBO) analysis is performed based on the B3LYP functional and the 6-311++G(d,p) basis set.

IV. EXPERIMENTAL RESULTS

As shown in Figure 2, the mass spectra of arabinose and mannose generated through the MALDI processes show that (arabinose-H)$^-$, (arabinose-H_2O)$^-$, (mannose-H)$^-$, and (mannose-H_2O)$^-$ are accessible features with (saccharide-H_2O)$^-$ as the most intense peak. Arabinose$^-$ parent anion can be also generated and detected, but mannose$^-$ parent anion is not observed in the present experiments. Their corresponding

DOI: 10.1021/acs.jpca.8b11838
J. Phys. Chem. A XXXX, XXX, XXX−XXX

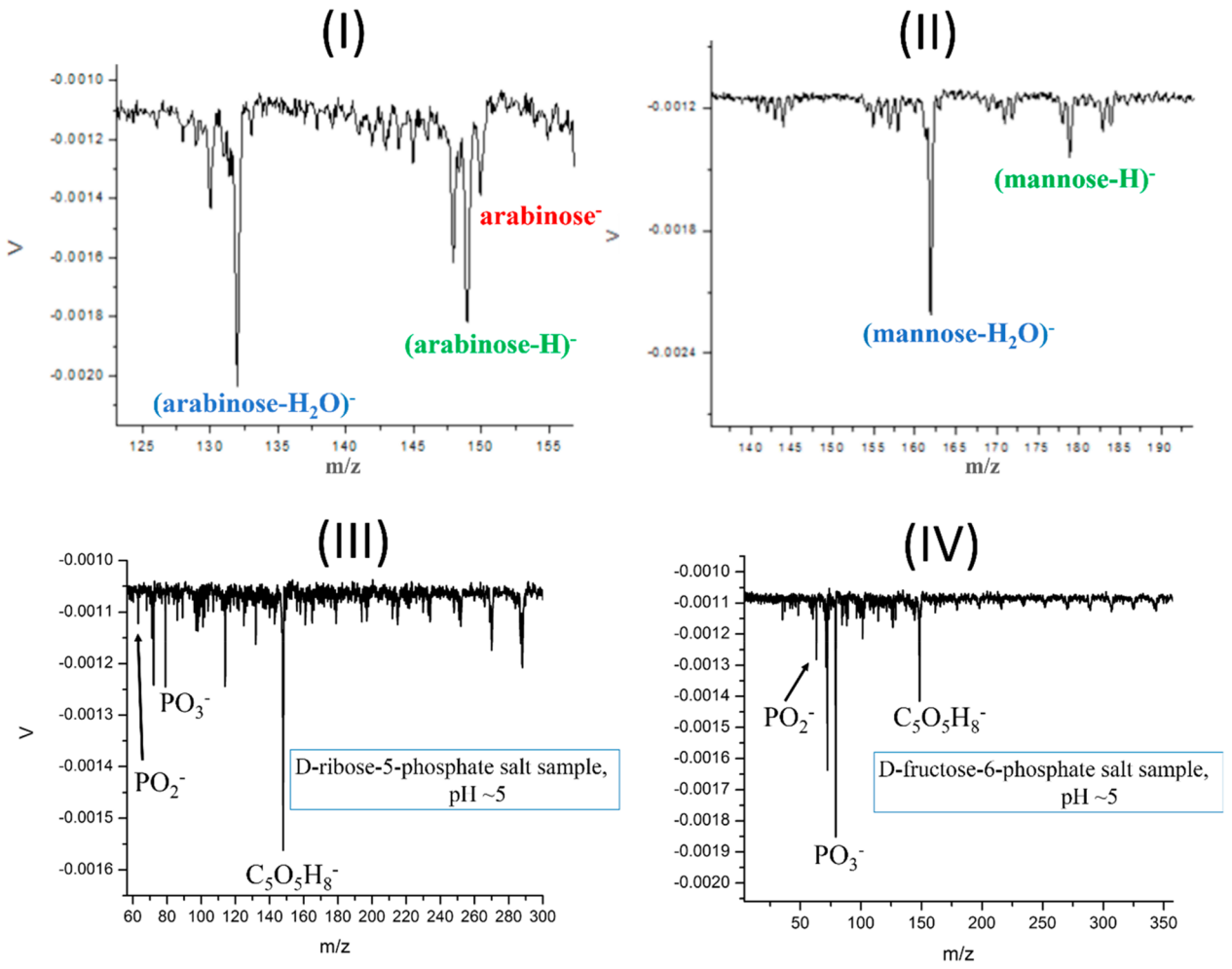

Figure 2. Mass spectra of arabinose (I), mannose (II), D-ribose-5-phosphate (III), and D-fructose-6-phosphate (IV) with sample (saccharide/DCM or saccharide phosphate/DCM) sprayed on a Zn substrate.

photoelectron spectra are displayed in Figure 3. VDEs are measured from the maxima of the corresponding PES peaks. The photoelectron spectrum of arabinose$^-$, recorded using 355 nm photons (Figure 3(I)), exhibits a feature centered at 1.67 eV. The photoelectron spectrum of (arabinose-H)$^-$ recorded with 266 nm photons, as can be seen from Figure 3 (II), shows a broad feature centered at around 2.82 eV up to above 4 eV. The broad feature can be contributed by different isomers. The photoelectron spectrum of (arabinose-H_2O)$^-$ recorded using 355 nm photons is displayed in Figure 3(III). It has two slightly distinguishable components centered at ~1.42 and ~1.90 eV. Similarly, the photoelectron spectrum of (mannose-H)$^-$, recorded using 266 nm photons (Figure 3(IV)), displays a broad feature centered at ~2.94 eV. Two slightly distinguished peaks centered at 2.25 and 1.61 eV are revealed in the photoelectron spectrum of (mannose-H_2O)$^-$, presented in Figure 3(V).

V. THEORETICAL RESULTS

The low energy isomers of arabinose$^-$, (arabinose-H)$^-$, (arabinose-H_2O)$^-$, mannose$^-$, (mannose-H)$^-$, and (mannose-H_2O)$^-$ anionic species, are summarized in Figures 4 to 9. More low energy isomers of (arabinose-H)$^-$, (arabinose-H_2O)$^-$, (mannose-H)$^-$, and (mannose-H_2O)$^-$ anions are summarized in Figures S5, S6, S8, and S9 in the Supporting Information. The isomers given in the main text figures are important and typical structures for each species and are discussed in the ensuing main text. Their calculated VDEs, relative energies, and comparison with experimentally determined values are summarized in Tables 1 and 2.

Arabinose. Five low energy isomers of arabinose$^-$ are presented in Figure 4. The lowest energy isomer arabinose$^-$ anion (A) has an open chain conformation, with a calculated VDE of 1.50 eV, in agreement with the experimental determination (1.67 eV). Isomer arabinose$^-$ anion (B) is nearly degenerate in energy with isomer (A), and also exhibits open chain structure but with different OH group orientations. Its theoretical VDE is 1.66 eV, in good agreement with the experiments. Conformational open chain isomer arabinose$^-$ anion (C) has a calculated VDE (1.21 eV) lower than the experimental observation. Furanose (D) and pyranose (E) isomers show much higher relative energies with respect to the lowest energy open chain structure and near zero theoretical VDEs (−0.13 and −0.11 eV). Thus, the photoelectron spectrum of arabinose$^-$ parent anion is mainly contributed by open chain isomers of arabinose$^-$ (A and B).

For (arabinose-H)$^-$, many low energy isomers are calculated: some of them are shown in Figure 5, with more isomers displayed in Figure S5. The most stable isomer (arabinose-H)$^-$ anion (A) can evolve from parent open chain structure with loss of H from the C atom at position (5) (labeled as (5C)H). Interestingly, it forms an H_2O unit

DOI: 10.1021/acs.jpca.8b11838
J. Phys. Chem. A XXXX, XXX, XXX−XXX

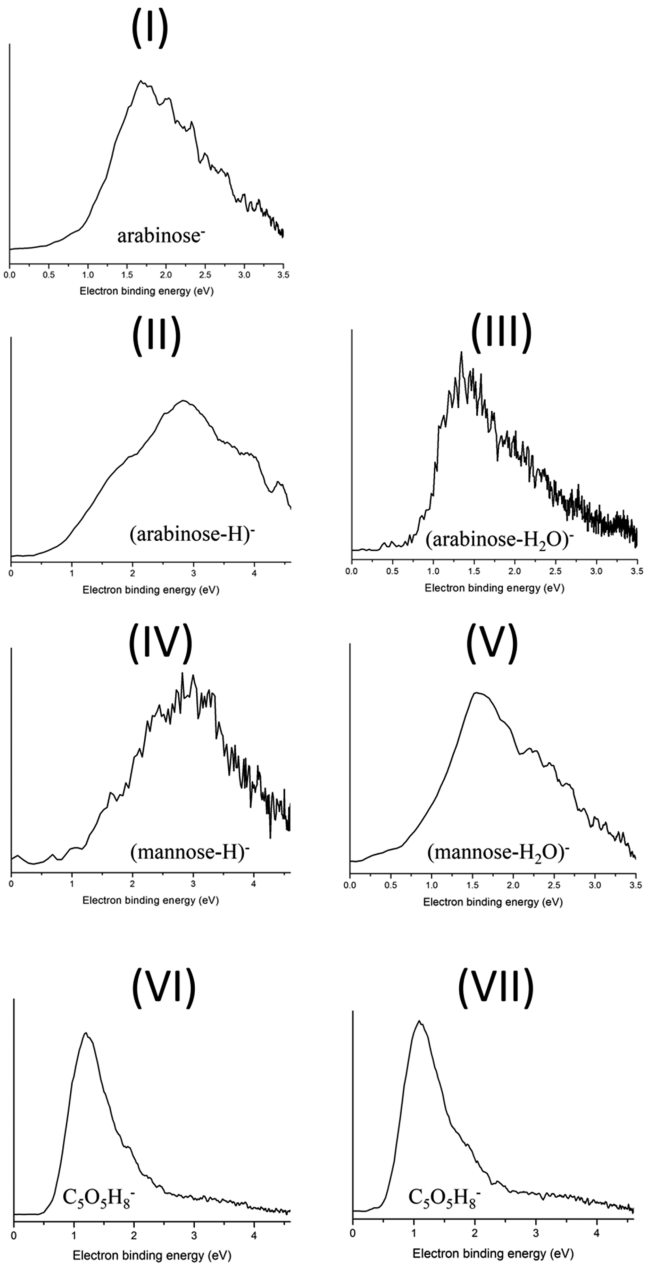

Figure 3. Photoelectron spectra of arabinose$^-$ (I), (arabinose-H)$^-$ (II), (arabinose-H_2O)$^-$ (III), (mannose-H)$^-$ (IV), and (mannose-H_2O)$^-$ (V) recorded with 355/266 nm photons, and photoelectron spectrum of $C_5O_5H_8^-$ recorded with 266 nm photons employing sample D-ribose-5-phosphate (VI) and D-fructose-6-phosphate (VII).

interacting with an oxygen through hydrogen bonding. The H_2O binding energy associated with isomer (arabinose-H)$^-$ (A) (open chain (B) − (5C)H) is calculated to be ∼14 kcal/mol (∼0.6 eV), larger than a single OH···O hydrogen bond. The theoretical VDE of (arabinose-H)$^-$ anion (A) is 3.52 eV, in the range of the broad PES feature of (arabinose-H)$^-$. Isomer (arabinose-H)$^-$ (B) anion has a furanose structure through losing an H from the O atom at (1) position (labeled as (1)H). It has a calculated VDE of 3.82 eV, as found in the experimental observations. Anion isomers (arabinose-H)$^-$ (C), (arabinose-H)$^-$ (D), (arabinose-H)$^-$ (E), (arabinose-H)$^-$ (F), and (arabinose-H)$^-$ (G) all have open chain conformations but with different detaching H positions, such as (2)H, (3)H, (2C)H, and (4C)H. Their VDEs are all calculated to be in the

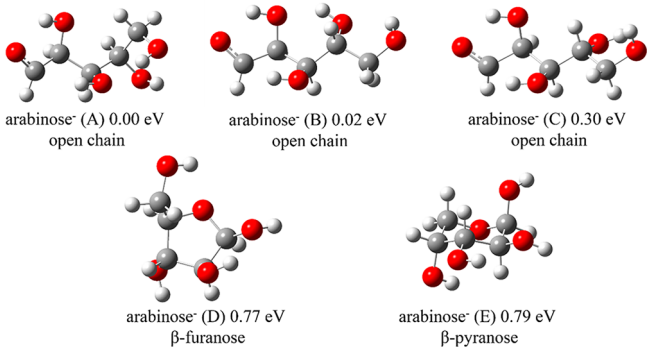

Figure 4. Optimized geometries of typical low energy anionic isomers of arabinose$^-$ based on B3LYP/6-311++G(d,p) calculations. The relative energies and structural polymorphs are indicated. The C atom order is the same as that in Figure 1. For open chain structures (1)C to (5)C is ordered from left to right. For both furanose and pyranose structures (1)C to (5)C is ordered from right to left in a clockwise direction.

Table 1. Relative Energies (Δ*E*) of the Low Energy Isomers of Arabinose-Related Anionic Species, and Comparison of their Calculated VDEs Based on a B3LYP/6-311++G(d,p) Algorithm[a]

		B3LYP/6-311++G(d,p)		
		Δ*E*	theor VDE	exptl VDE
arabinose$^-$	arabinose$^-$ (A)	0.00	1.50	1.67
	arabinose$^-$ (B)	0.02	1.66	
	arabinose$^-$ (C)	0.30	1.21	
	arabinose$^-$ (D)	0.77	−0.13	
	arabinose$^-$ (E)	0.79	−0.11	
(arabinose-H)$^-$	(arabinose-H)$^-$ (A)	0.00	3.52	∼2.82
	(arabinose-H)$^-$ (B)	0.39	3.82	
	(arabinose-H)$^-$ (C)	0.40	4.51	
	(arabinose-H)$^-$ (D)	0.45	4.07	
	(arabinose-H)$^-$ (E)	0.52	3.96	
	(arabinose-H)$^-$ (F)	0.53	2.62	
	(arabinose-H)$^-$ (G)	0.56	2.50	
	(arabinose-H)$^-$ (H)	0.63	3.92	
	(arabinose-H)$^-$ (I)	0.65	3.50	
(arabinose-H_2O)$^-$	(arabinose-H_2O)$^-$ (A)	0.00	2.90	
	(arabinose-H_2O)$^-$ (B)	0.13	2.63	
	(arabinose-H_2O)$^-$ (C)	0.21	3.06	
	(arabinose-H_2O)$^-$ (D)	0.22	1.95	∼1.90
	(arabinose-H_2O)$^-$ (E)	0.30	1.97	
	(arabinose-H_2O)$^-$ (F)	0.68	1.50	∼1.42

[a]Experimental measurements are in the right hand column. All energies are in eV.

range of the broad experimental PES feature. (arabinose-H)$^-$ (F) and (arabinose-H)$^-$ (G) have calculated VDEs of 2.62 and 2.50 eV, in excellent agreement with the lower EBE portion of the broad PES feature. Isomers (arabinose-H)$^-$ F and G lose H from the 2C position without obvious structural change compared to the parent species. They have higher relative energy (>0.53 eV) than the lowest energy isomer with loss of H from C atom but with significant structural change by forming an H_2O unit. Anion isomers (arabinose-H)$^-$ (H) and (arabinose-H)$^-$ (I) can develop from cyclic (furanose and pyranose) structures with loss H from position (1). Thus, the

DOI: 10.1021/acs.jpca.8b11838
J. Phys. Chem. A XXXX, XXX, XXX−XXX

Table 2. Relative energies (ΔE) of the low energy isomers of mannose related anionic species, and comparison of their calculated VDEs based on a B3LYP/6-311++G(d,p) algorithm[a]

		B3LYP/6-311++G(d,p)		
		ΔE	theor VDE	exptl VDE
mannose$^-$	mannose$^-$ (A)	0.00	0.84	—
	mannose$^-$ (B)	0.24	0.77	
	mannose$^-$ (C)	0.47	0.33	
	mannose$^-$ (D)	0.58	−0.08	
	mannose$^-$ (E)	0.63	−0.09	
(mannose-H)$^-$	(mannose-H)$^-$ (A)	0.00	4.32	∼2.94
	(mannose-H)$^-$ (B)	0.05	3.84	
	(mannose-H)$^-$ (C)	0.21	4.43	
	(mannose-H)$^-$ (D)	0.25	4.28	
	(mannose-H)$^-$ (E)	0.38	4.24	
	(mannose-H)$^-$ (F)	0.56	4.25	
	(mannose-H)$^-$ (G)	0.85	3.48	
	(mannose-H)$^-$ (H)	0.88	3.57	
	(mannose-H)$^-$ (I)	1.26	3.15	
(mannose-H_2O)$^-$	(mannose-H_2O)$^-$ (A)	0.00	2.30	∼2.25
	(mannose-H_2O)$^-$ (B)	0.03	1.91	
	(mannose-H_2O)$^-$ (C)	0.03	1.50	1.61
	(mannose-H_2O)$^-$ (D)	0.64	1.11	
	(mannose-H_2O)$^-$ (E)	0.68	4.09	
	(mannose-H_2O)$^-$ (F)	0.68	4.30	

[a]Experimental measurements are at the right hand column. All energies are in eV.

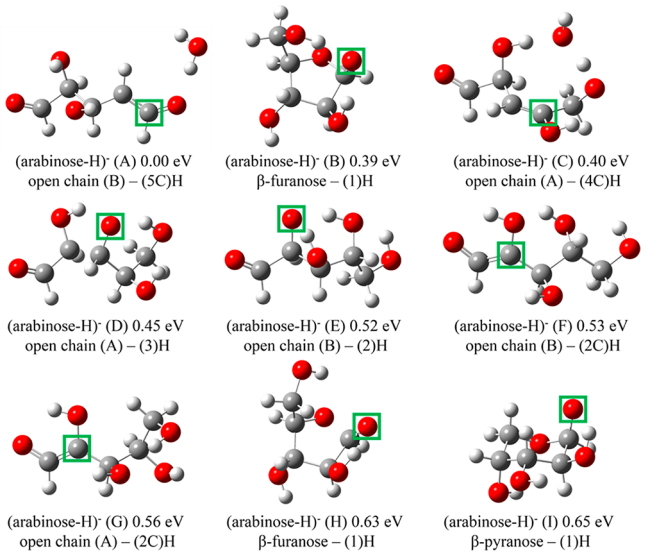

Figure 5. Optimized geometries of typical low energy anionic isomers of (arabinose-H)$^-$ based on B3LYP/6-311++G(d,p) calculations. The relative energies and structural polymorphs are indicated. The green square indicates loss of hydrogen at the indicated position. The C atom order is the same as that in Figure 1. For open chain structures (1)C to (5)C is ordered from left to right. For both furanose and pyranose structures (1)C to (5)C is ordered from right to left in a clockwise direction.

broad feature in the photoelectron spectrum of (arabinose-H)$^-$ anion is contributed by open chain structures with loss of H from an O or C atom at different positions, in addition to pyranose and furanose structures with loss of H from an O atom mostly at position 1. These isomeric forms of (arabinose-H)$^-$ anion are both positional and conformational in nature. There are more cyclic and open chain isomers losing H from a C atom with high relative energies (>2 eV), shown in the Supporting Information. They have smaller calculated VDEs (∼1.8 eV) and they can be identified to contribute to the small shoulder part of PES feature for (arabinose-H)$^-$. They are likely to be present in the experiments even at such high relative energies: ion generation processes could overcome the respective local energy barriers, enabling these species to form as different local isomers. Geometries of these saccharide molecules are apparently quite flexible.

The typical low energy isomers of (arabinose-H_2O)$^-$ anion are presented in Figure 6: the green squares on the structures indicate loss of H and the green circles indicate loss of an OH group at the identified positions. They all evolve from open chain conformations. Anion isomers (arabinose-H_2O)$^-$ (A and B) evidence loss of H from position 2 and loss of OH from position 5 with C−C bond rupture. Their calculated VDEs are 2.90 and 2.63 eV, respectively, higher than the experimental values. Isomer anion (arabinose-H_2O)$^-$ (C) loses H from position 2 and OH from position 4, but its calculated VDE is higher than the experimental one: they must have very low population in the experimental sample. Isomer (arabinose-H_2O)$^-$ (D) undergoes loss of H from position 5C and loss of OH from position 3. Anion isomer (arabinose-H_2O)$^-$ (E) exhibits the same positional character ((5C)H/(3)OH) as isomer (arabinose-H_2O)$^-$ (D), but with conformational differences. They both form an H_2O unit in the fragment species. The theoretical VDEs of anion isomers D and E are 1.95 and 1.97 eV, in excellent accord with the high EBE portion of the experimental feature (1.90 eV). Anion isomer (arabinose-H_2O)$^-$ (F) has (2C)H/(3)OH loss positions: its calculated VDE (1.50 eV) is in good agreement with the low EBE side of the experimental feature (1.42 eV). Thus, anion isomers (arabinose-H_2O)$^-$ (D and E) contribute to the higher EBE components of the broad PES peak in the spectrum of (arabinose-H_2O)$^-$, while the (arabinose-H_2O)$^-$ (F) anion form contributes to the lower energy EBE component of this feature.

Mannose. Mannose$^-$ parent anion is not detected in the present RTOFMS/PES experiments. The calculated typical low energy isomers of mannose$^-$ anion are shown in Figure 7. The lower energy isomers evidence open chain conformations with positive calculated VDEs, identical to the situation for arabinose$^-$ anion. Cyclic (furanose and pyranose) anionic structures have higher energies than those of the open chain ones and near zero calculated VDEs.

The typical low energy isomers of (mannose-H)$^-$ anions are displayed in Figure 8. The most stable of these is an open chain conformation derived by losing H from position (5C) and forming an H_2O unit. Its calculated VDE of 4.32 eV is in the tail of experimental broad PES feature. Anion isomer (mannose-H)$^-$ (B) also exhibits an open chain structure with loss of H from (3C) position: its theoretical VDE of 3.84 eV is in the range of broad PES feature. Anion isomers (mannose-H)$^-$ (C), (mannose-H)$^-$ (D), (mannose-H)$^-$ (E), and (mannose-H)$^-$ (F) have cyclic structures and lose H from 4C, 3, 1, and 2 positions, respectively. Their calculated VDEs are all in the tail of the broad PES feature. Anion isomers (mannose-H)$^-$ (G), (mannose-H)$^-$ (H), and (mannose-H)$^-$ (I) are open chain conformations with loss of from positions 3, 4, and 2: their theoretical VDEs are calculated to be 3.48, 3.57,

DOI: 10.1021/acs.jpca.8b11838
J. Phys. Chem. A XXXX, XXX, XXX−XXX

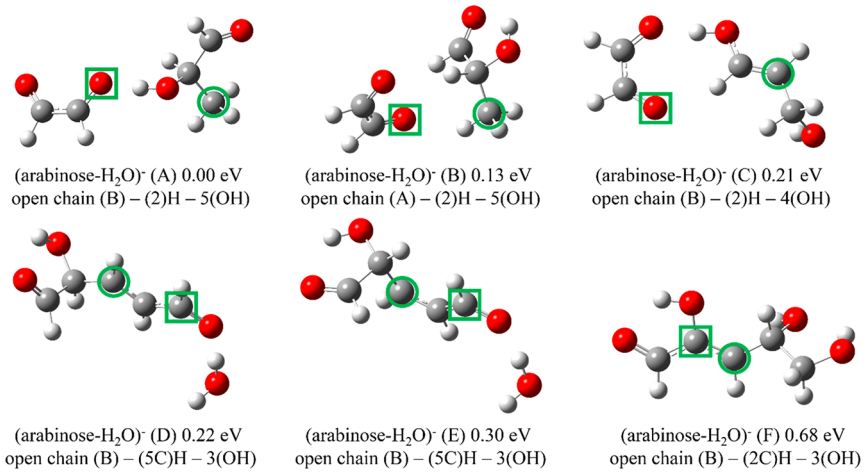

Figure 6. Optimized geometries of typical low energy anionic isomers of $(\text{arabinose-H}_2\text{O})^-$ based on B3LYP/6-311++G(d,p) calculations. The relative energies and structural polymorphs are indicated. The C atom numberings are the same as those in Figure 1. For open chain structures, (1)C to (5)C is ordered from left to right. For both furanose and pyranose structures, (1)C to (5)C is ordered from right to left in a clockwise direction.

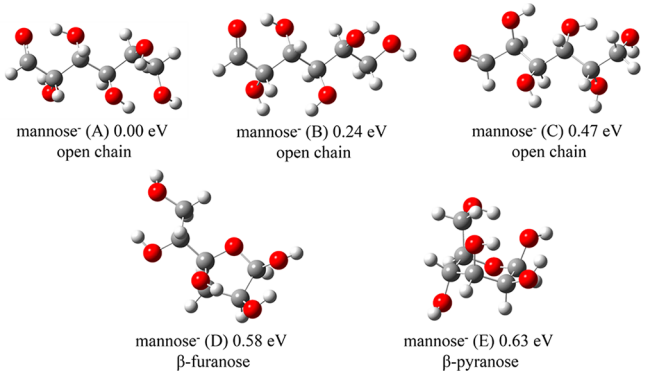

Figure 7. Optimized geometries of typical low energy anionic isomers of mannose$^-$ based on B3LYP/6-311++G(d,p) calculations. The relative energies and structural polymorphs are indicated. The C atom order is the same as that in Figure 1. For open chain structures, (1)C to (5)C is ordered from left to right. For both furanose and pyranose structures, (1)C to (5)C is ordered from right to left in a clockwise direction.

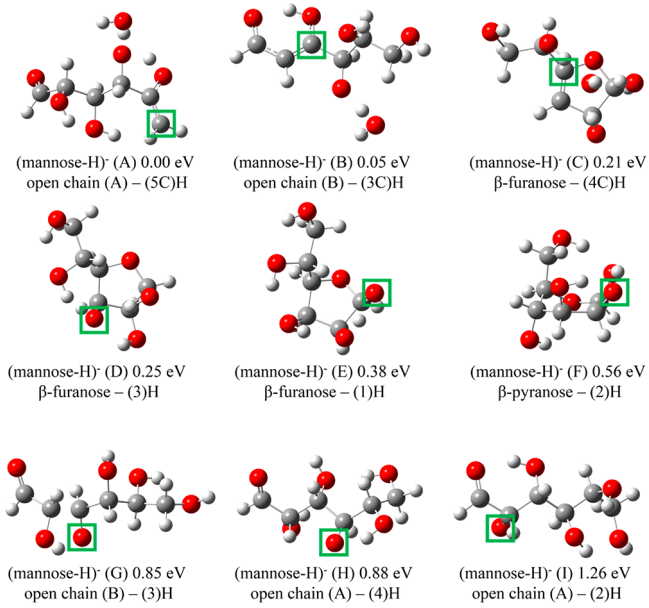

Figure 8. Optimized geometries of typical low energy anionic isomers of $(\text{mannose-H})^-$ based on B3LYP/6-311++G(d,p) calculations. The relative energies and structural polymorphs are indicated. The green square indicates loss of hydrogen at the indicated position. The C atom order is the same as that in Figure 1. For open chain structures, (1)C to (5)C is ordered from left to right. For both furanose and pyranose structures, (1)C to (5)C is ordered from right to left in a clockwise direction.

and 3.15 eV, respectively, in the range of broad experimental feature. Isomers $(\text{mannose-H})^-$ (G), $(\text{mannose-H})^-$ (H), and $(\text{mannose-H})^-$ (I) mostly contribute to the major EBE portion of broad PES feature for $(\text{mannose-H})^-$. These open chain structures are more likely to be present in the experiments even with higher relative energies, since minus H species can evolve from parent anion (parent anion is not observed and must undergo dissociation), and lower energy open chain parent anion species are more likely to be populated than higher energy cyclic parent anions. Thus, the photoelectron spectrum of $(\text{mannose-H})^-$ arises from many conformational and positional isomers that coexist in the experimental sample.

The typical low energy isomers for anion $(\text{mannose-H}_2\text{O})^-$ are shown in Figure 9: they are all derived from open chain structures, identical to those of $(\text{arabinose-H}_2\text{O})^-$. Anion isomers $(\text{mannose-H}_2\text{O})^-$ (A and B) are nearly energetically degenerate. They both arise through loss of H from position 6 and loss OH from position 4, but with conformational difference. C−C bond rupture and H_2O unit formation occur in these two isomers. The calculated VDEs of anionic isomers (A) and (B) are 2.30 and 1.91 eV and are in good agreement with the higher EBE side of the experimental PES feature (~2.25 eV). Anionic isomer $(\text{mannose-H}_2\text{O})^-$ (C) loses H from position 4 and OH from position 2 with C−C bond rupture: its calculated VDE (1.50 eV) is in good agreement with the lower EBE side of PES feature (1.61). Anionic isomer $(\text{mannose-H}_2\text{O})^-$ (D) also exhibits (4)H/(2)(OH) positional losses: it has a theoretical VDE of 1.11 eV, lower than the experimental VDE determination. Anion isomers $(\text{mannose-H}_2\text{O})^-$ (E) and $(\text{mannose-H}_2\text{O})^-$ (F) have different dissociation positions from those of the lower energy isomers. Their calculated VDEs are determined to be 4.09 and 4.30 eV, obviously higher than the experimental

DOI: 10.1021/acs.jpca.8b11838
J. Phys. Chem. A XXXX, XXX, XXX−XXX

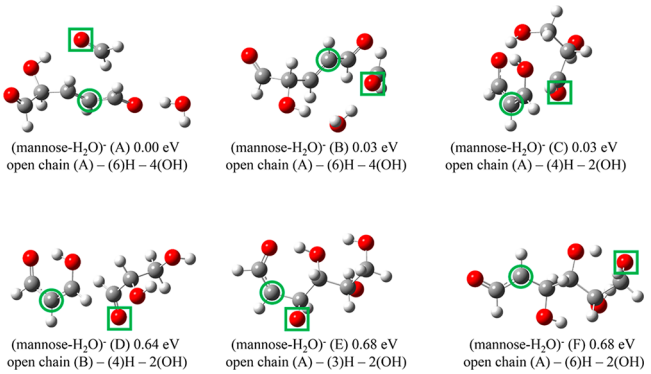

Figure 9. Optimized geometries of typical low energy anionic isomers of $(\text{mannose-H}_2\text{O})^-$ based on B3LYP/6-311++G(d,p) calculations. The relative energies and structural polymorphs are indicated. The green square indicates loss of hydrogen at the indicated position. The C atom order is the same as that in Figure 1. For open chain structures, (1)C to (5)C is ordered from left to right. For both furanose and pyranose structures, (1)C to (5)C is ordered from right to left in a clockwise direction.

observation. Isomers $(\text{mannose-H}_2\text{O})^-$ (E and F) are less likely to be populated in the experimental sample. Thus, two positional types ((6)H/(4)(OH) and (4)H/(2)(OH)) of isomers are expected to contribute to the two EBE components of the photoelectron spectrum of $(\text{mannose-H}_2\text{O})^-$.

VI. DISCUSSION

The arabinose parent anion is observed in the TOFMS: through the PES measured VDEs, arabinose parent anion is assigned to exist as the lowest energy open chain structure. From an NBO analysis, as can be seen from Figure 10, the

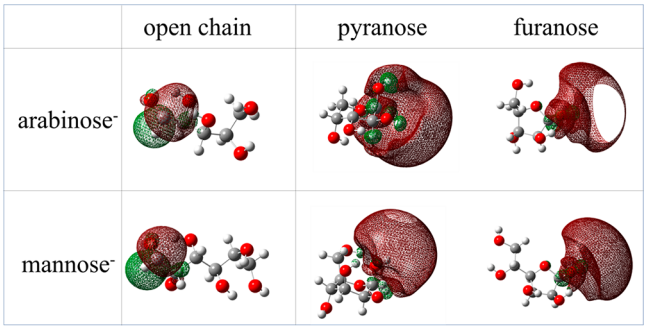

Figure 10. NBO/HOMOs (highest occupied molecular orbitals) of open chain and cyclic structures of arabinose$^-$ and mannose$^-$ parent anions from an NBO analysis based on B3LYP/6-311++G(d,p) DFT calculations. Open chain structures of the two parent anions both show valence bound characters on a p orbital of the carbonyl C atom. Cyclic structures of two parent anions both display dipole bound character with the added electron distributing around H atoms.

highest singly occupied molecular orbitals (HSOMO) of open chain structures of the two anionic parent species are mostly located on a p orbital of a carbonyl C atom. The HSOMO of cyclic (pyranose and furanose) anions display a dipole bound character with the added electron distributed around H atoms. Both of these saccharides evidence H and H_2O cleavage dissociation anions. Many positional anionic isomers of $(\text{saccharide-H})^-$ with conformational differences are identified to be present in the experimental sample, while only two positional isomers are assigned for $(\text{saccharide-H}_2\text{O})^-$.

The RNA/DNA backbone sugar constituent natural selection choice can be further addressed in the present studies based on the RTOFMA/PES/DFT results for ribose,[2] mannose, arabinose, and fructose.[1] The sugar constituent structure of the RNA backbone presents a cyclic furanose structure, only cyclic furanose structures are discussed for consideration of the natural selection choice. On the basis of the summary of identified and observed ions for the four sugar molecule related anionic species given in Table 3, cyclic

Table 3. Anionic Species Observed and Identified through the RTOFMS/PES/DFT System[a]

	SAC^-	$(SAC\text{-}H)^-$	$(SAC\text{-}OH)^-$	$(SAC\text{-}H_2O)^-$
ribose		$(R_{cy}\text{-}H)^-$ $(R_{oc}\text{-}H)^-$		$(R_{oc}\text{-}H_2O)^-$
mannose		$(M_{cy}\text{-}H)^-$ $(M_{oc}\text{-}H)^-$		$(M_{oc}\text{-}H_2O)^-$
arabinose	A_{oc}^-	$(A_{cy}\text{-}H)^-$ $(A_{oc}\text{-}H)^-$		$(A_{oc}\text{-}H_2O)^-$
fructose	F_{oc}^-	$(F_{cy}\text{-}H)^-$ $(F_{oc}\text{-}H)^-$	$(F_{oc}\text{-}OH)^-$	$(F_{oc}\text{-}H_2O)^-$

[a] SAC_{cy}^- indicates cyclic structure, SAC_{oc}^- indicates open chain structure.

furanose structures are only accessible for the $(\text{saccharide-H})^-$ species. The possible reaction mechanism/kinetic processes for forming cyclic furanose $(\text{saccharide-H})^-$ are shown in Figure 11. Cyclic neutral parent species can capture an extra electron

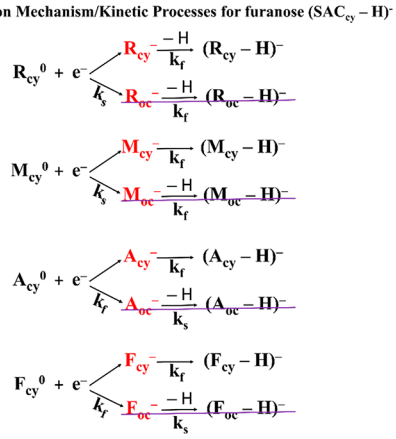

Figure 11. Reaction mechanism/kinetic processes for furanose $(SAC_{cy} - H)^-$. SAC_{cy}^- (cyclic structure, dipole bound e^- not stable); SAC_{oc}^- (open chain structure, valence bound e^- stable), but not observed for ribose and mannose. Purple line indicates path not viable.

first to form an unstable intermediate parent anion. Such a cyclic intermediate parent anion can dissociate an H atom rapidly to form furanose $(\text{saccharide-H})^-$ anions. The intermediate cyclic parent anion can also undergo ring-opening to form open chain parent anions, which can continue to lose an H atom to form open chain $(\text{saccharide-H})^-$ anions. Different kinetic rates can be suggested for ring-opening with regard to further dissociation reaction pathways. For instance, since arabinose$^-$ and fructose$^-$ parent open chain anionic species are detected, but not those of ribose$^-$ and mannose$^-$,

DOI: 10.1021/acs.jpca.8b11838
J. Phys. Chem. A XXXX, XXX, XXX–XXX

arabinose and fructose anions should have faster kinetics for ring-opening than ribose and mannose anions do. Thereby, arabinose and fructose anions are less stabilizing for RNA preservation than ribose$^-$ and mannose$^-$ anions are under UVU/e$^-$, reducing conditions. Since only cyclic furanose structures are considered for RNA preservation, ring-opening pathways are no longer considered.

The relative energies of cyclic furanose (saccharide-H)$^-$ species with respect to their corresponding lowest energy structures or their lowest energy furanose structures for the four saccharides under consideration are summarized in Figure 12. Note that these relative energies for (ribose-H)$^-$ and

		ΔE (eV)[a]	ΔE (eV)[b]
furanose (ribose – H)$^-$	isomer (I)	0.27	0.00
	isomer (II)	0.27	0.00
furanose (mannsoe – H)$^-$	isomer (I)	0.21	0.00
	isomer (II)	0.25	0.04
furanose (arabinose – H)$^-$	isomer (I)	0.39	0.00
	isomer (II)	0.63	0.24
furanose (fructose – H)$^-$	isomer (I)	0.63	0.00
	isomer (II)	0.85	0.22

Figure 12. Relative energies of furanose (saccharide-H)$^-$ with respect to the lowest energy isomers[a] and the lowest energy furanose isomers[b] of (saccharide-H)$^-$.

(mannose-H)$^-$ are smaller compared to those for (arabinose-H)$^-$ and (fructose-H)$^-$. Arabinose and fructose can thereby additionally be eliminated from the natural selection process for energy considerations, since they are energetically less likely to form (arabinose-H)$^-$ and (fructose-H)$^-$ and less likely to revert back to an appropriate neutral species.

Furanose (saccharide-H)$^-$ species can revert to form parent neutral by first losing an excess electron or by first binding an H atom, as represented in Figure 13. In comparing the process

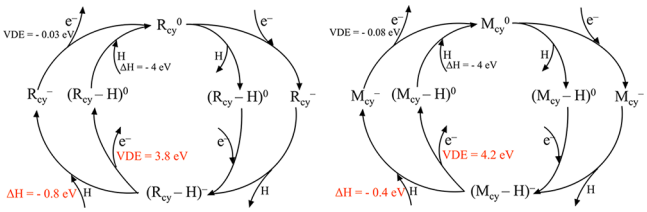

Figure 13. Reaction mechanism/kinetic processes from furanose (saccharide-H)$^-$ to furanose saccharide neutral.

from furanose (saccharide-H)$^-$ to furanose neutral saccharide, note that the electron binding energy (3.8 eV) of furanose (ribose-H)$^-$ is smaller than that (4.2 eV) of furanose (mannose-H)$^-$ and that the H binding energy (0.8 eV) of furanose (ribose-H)$^-$ is greater than that (0.4 eV) of furanose (mannose-H)$^-$. Furanose (ribose-H)$^-$ is thereby more likely to form furanose neutral ribose than (mannose-H)$^-$ is to form furanose mannose neutral. Thereby ribose can be considered to be better than mannose for protection of RNA.

Saccharide phosphates (D-ribose-5-phosphate and D-fructose-6-phosphate, Figure 14) have also been considered for natural selection issues. From an NBO analysis (depicted in

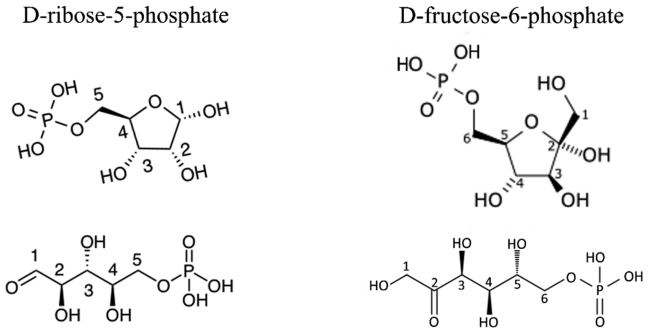

Figure 14. Schematic structures of D-ribose-5-phosphate (left) and D-fructose-6-phosphate (right).

Figure 15), the HSOMOs of D-ribose-5-phosphate and D-fructose-6-phosphate parent anions show that open chain

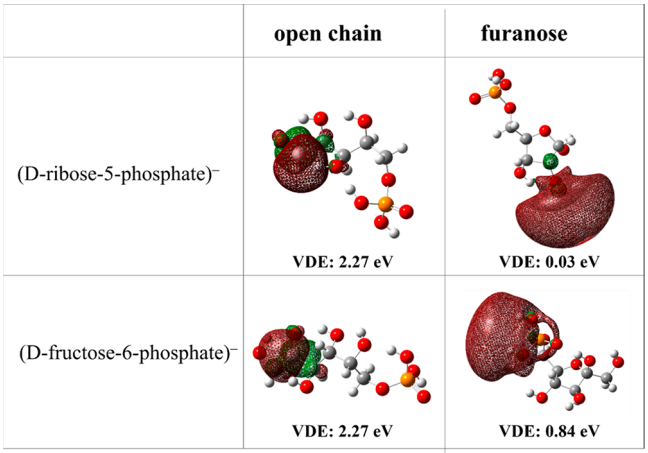

Figure 15. NBO/HOMOs (highest occupied molecular orbitals) of D-ribose-5-phosphate and D-fructose-6-phosphate parent anions from an NBO analysis based on B3LYP/6-311++G(d,p) DFT calculations. Open chain structures of two parent anions both show valence bound characters mostly on a p orbital of the carbonyl C atom. The furanose structure of D-ribose-5-phosphate parent anion displays dipole bound character with the added electron distributed around H atoms of the sugar moiety, while D-fructose-6-phosphate parent anion has the dipole bound electron mostly localized on H atoms of the phosphate group.

structures evidence valence bound character mostly in a p orbital of the carbonyl C atom. The furanose structure of D-ribose-5-phosphate parent anion displays dipole bound distribution with the added electron distributed around H atoms of the sugar moiety, while D-fructose-6-phosphate parent anion has the dipole bound electron mostly localized on H atoms of the phosphate group. The phosphate group thus has only a minor effect on the electronic structure of ribose (Figure 7 in ref 2).

An additional dissociation ion ($C_5O_5H_8^-$) is observed in the mass spectra of both D-ribose-5-phosphate and D-fructose-6-phosphate (see Figure 2(III and IV)). The corresponding photoelectron spectrum of $C_5O_5H_8^-$ from D-ribose-5-phosphate, as shown in Figure 3(VI), evidence a feature centered at around 1.22 eV. Similarly, the photoelectron spectrum of $C_5O_5H_8^-$ from D-fructose-6-phosphate (Figure 3(VII)) shows a peak only slightly red-shifted (~0.10 eV) from 1.22 eV. On the basis of the reasonable agreement between the

DOI: 10.1021/acs.jpca.8b11838
J. Phys. Chem. A XXXX, XXX, XXX−XXX

experimental VDEs and calculated VDEs, two anionic structures of $C_5O_5H_8^-$ can be assigned as shown in Figure 16. $C_5O_5H_8^-$ can evolve from D-ribose-5-phosphate by loss of a

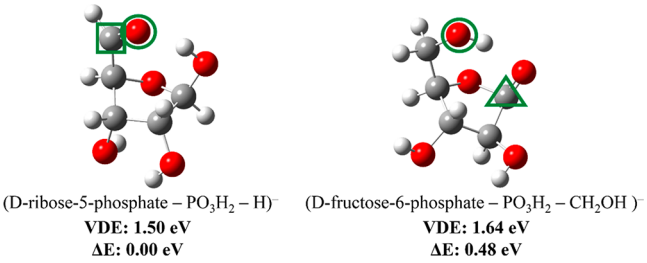

Figure 16. Optimized geometries of $C_5O_5H_8^-$ based on B3LYP/6-311++G(d,p) calculations for D-ribose-5-phosphate (left) and D-fructose-6-phosphate (right), respectively. The relative energies and calculated VDEs are indicated. The green circle marks loss of dihydrogen phosphite group (PO_3H_2) at the indicated position. The green square marks loss of H at the indicated position. The green triangle marks loss of CH_2OH moiety at the indicated position.

dihydrogen phosphite group and an H atom; it can also develop from D-fructose-6-phosphate with loss of dihydrogen phosphite group and a CH_2OH moiety. Since fission of the CH_2OH moiety from the fructose phosphate can damaged the sugar moiety, fructose is suggested to be less protective than ribose for the genetic molecules.

Preliminary calculations have also been explored for the diphosphates of both fructose and ribose in the furanose structure only. These results, at the ωB97XD/aug-cc-pvtz level, show that for both saccharide diphosphates the added electron is only dipole bound to the phosphate H atoms.

VII. CONCLUSIONS

VII.1. Arabinose- and Mannose-Related Species. Arabinose and mannose related anionic species generated through the MALDI process are investigated by employing negative ion PES in conjunction with DFT calculations. The VDEs of the various anionic species are determined experimentally, and the corresponding structures can be assigned based on the good agreement between experimental and calculated VDEs.

Isolated, gas phase arabinose parent anion is observed in the arabinose mass spectrum; it is identified through DFT calculations to exit as open chain structures. The mannose parent anion is not observed. Open chain structures for both parent anions are the lowest energy isomers with a valence bound excess electron. Both cyclic pyranose and furanose parent anions have higher relative energy than their corresponding open chain isomers. These latter cyclic anions have only a dipole bound extra electron with very low VDEs.

Dissociation anions with loss of H and H_2O are detected for the two saccharide molecules. Many conformational and positional isomers of (arabinose-H)$^-$ and (mannose-H)$^-$ are predicted and observed to coexist in the experiments: these species contribute to their broad photoelectron spectra. The lowest energy open chain and cyclic (pyranose and furanose) isomers of arabinose$^-$ lose H from the 5C and 1 positions, respectively. Mannose$^-$ appears to dissociate H from 5C for the lowest energy open chain isomer, from 4C for the lowest energy furanose isomer, and from 2 for the lowest energy pyranose isomer.

Two types of positional isomers are identified to contribute to the experimental PES of (arabinose-H_2O)$^-$ and (mannose-H_2O)$^-$: they contribute to the higher and lower EBE components of the broad (saccharide-H_2O)$^-$ feature. These positional isomers are all derived from open chain structures. Each positional isomer exhibits conformational differences. (arabinose-H_2O)$^-$ isomers have (5C)H/(3)OH and (2C)H/(3)OH dissociation positions with respect to the parent arabinose anion. (mannose-H_2O)$^-$ isomers have (6)H/(4)OH and (4)H/(2)OH dissociation positions with respect to the parent mannose anion.

The calculated enthalpy change (ΔH) for reactions from parent species (both anion and neutral) to (saccharide-H_2O)$^-$ through loss of one water molecule directly, has been previously determined to be negative: both reactions are therefore thermodynamically allowed. Therefore, (saccharide-H_2O)$^-$ species can be generated either from the MALDI/ablation processes themselves or from dehydration reaction pathways from the parent species through loss of one H_2O molecule directly. The fixed positions for loss of H_2O to form (saccharide-H_2O)$^-$ anions, different from the situation for loss of one H for (saccharide-H)$^-$ anions, also suggests direct, spontaneous processes for loss of water.

VII.2. Comparison of the Four Sugar Molecule (Ribose, Mannose, Arabinose, and Fructose) Results and Discussion of Ribose Natural Selection. On the basis of the anions observed and identified through the same PES/DFT techniques and apparatus for the four saccharides (ribose, mannose, arabinose and fructose), the rational for natural selection of ribose as the sugar backbone constituent in RNA can be explored. The factors that contribute to the evolutionary choice of ribose over other saccharides as the backbone support for genetic related molecules have previously been focused on size and steric bulk effects. Under the present analysis, ion and neutral electronic structures are considered for the unique evolutionary selection of ribose. This matter is now examined with regard to protection/preservation of RNA/DNA under reducing/ionizing conditions of VUV radiation/electron capture damage.

Since the sugar moiety presents a furanose cyclic structure for the DNA/RNA backbone support and cyclic structures are only accessible in (saccharide-H)$^-$ species, only cyclic furanose species are considered for the RNA/DNA stability. Cyclic furanose (saccharide-H)$^-$ structures can evolve from furanose parent neutrals by attaching an extra electron to form an intermediate anionic state, which quickly loses an H. Furanose neutral species can also undergo ring-opening after capturing an excess electron. Open chain ribose and mannose anionic species are not observed, but instead open chain arabinose and fructose parent anions are detected. This fact suggests that furanose arabinose and fructose parent anions appear to ring open relatively faster than furanose ribose and mannose do. Thus, arabinose and fructose are less likely to have been evolutionarily advantageous for preservation of RNA.

The relative energies of furanose (ribose-H)$^-$ and (mannose-H)$^-$ with respect to their corresponding lowest energy isomers are smaller than those of furanose (arabinose-H)$^-$ and (fructose-H)$^-$. Thereby, arabinose and fructose can also be eliminated from the natural selection processes based on energy consideration. Note that the ablation/supersonic expansion process gives lower lying states—all saccharides related species should have similar cooling conditions.

DOI: 10.1021/acs.jpca.8b11838
J. Phys. Chem. A XXXX, XXX, XXX−XXX

Anionic furanose (saccharide-H)$^-$ species can be considered to form parent neutrals by first losing an excess electron or binding H atom. Since furanose (ribose-H)$^-$ has a smaller excess electron binding energy and a greater H binding energy than furanose (mannose-H)$^-$ does, furanose (ribose-H)$^-$ can form neutral ribose more readily than (mannose-H)$^-$ can form neutral mannose. From the point of view of RNA preservation, ribose seems better than mannose, based on the above anionic/neutral electronic properties.

VII.3. Saccharide Phosphates. The DNA/RNA backbone consists of a sugar moiety and a phosphate moiety, in addition to the central aromatic nitrogenous bases. Saccharide phosphates (D-ribose-5-phosphate and D-fructose-6-phosphate) are investigated and compared for further understanding of the natural selection of ribose as the sugar constituent in RNA. No parent anion or dissociation ions with loss of H, OH or H_2O are observed in the mass spectra of the two saccharide phosphate samples obtained through the MALDI method. Significant dissociation ions PO_2^-, PO_3^-, and an anion with formula of $C_5O_5H_8^-$ are accessible in both mass spectra of D-ribose-5-phosphate and D-fructose-6-phosphate. NBO/HSOMOs of open chain anionic structures of the two parent anions are analyzed and exhibit a valence bound extra electron also mostly on a p orbital of a carbonyl C atom. The furanose cyclic anionic D-ribose-5-phosphate form has a dipole bound character with the added electron distributed around H atoms of the sugar moiety. The furanose anionic structure of D-fructose-6-phosphate has its dipole bound excess electron mostly localized on the H atoms of the phosphate group. This suggests that the phosphate group does not change the electronic nature of the ribose moiety in RNA.

$C_5O_5H_8^-$ anion can evolve from D-ribose-5-phosphate via losing dihydrogen phosphite group first then continuing to lose H. In order to form $C_5O_5H_8^-$, D-fructose-6-phosphate loses dihydrogen phosphite group first then loses a CH_2OH group, which damages the sugar moiety. Ribose can thereby again be more protective than fructose for RNA in a highly VUV/e$^-$ environment.

■ ASSOCIATED CONTENT

Supporting Information

The Supporting Information is available free of charge on the ACS Publications website at DOI: 10.1021/acs.jpca.8b11838.

More low-lying isomers of (arabinose-H)$^-$, (arabinose-H_2O)$^-$, (mannose-H)$^-$, and (mannose-H_2O)$^-$ anions (PDF)

■ AUTHOR INFORMATION

Corresponding Author

*(E.R.B.) E-mail: erb@colostate.edu.

ORCID

Elliot R. Bernstein: 0000-0003-0045-7193

Notes

The authors declare no competing financial interest.

■ ACKNOWLEDGMENTS

This work is supported by a grant from the US Air Force Office of Scientific Research (AFOSR) through Grant Number FA9550-10-1-0454, the National Science Foundation (NSF) ERC for Extreme Ultraviolet Science and Technology under NSF Award No. 0310717, the Army Research Office (ARO, Grant Nos. FA9550-10-1-0454 and W911-NF13-10192), and a DoD DURIP grant (W911NF-13-1-0192).

■ REFERENCES

(1) Zeng, Z.; Bernstein, E. R. Anionic fructose-related conformational and positional isomers assigned through PES experiments and DFT calculations. *Phys. Chem. Chem. Phys.* **2017**, *19*, 23325−23344.

(2) Zeng, Z.; Bernstein, E. R. Anionic ribose related species explored through PES experiments, DFT calculations, and through comparison with anionic fructose species. *Phys. Chem. Chem. Phys.* **2017**, *19*, 28950−28962.

(3) Bauer, W. D.; Talmadge, K. W.; Keegstra, K.; Albersheim, P. The structure of plant cell walls. *Plant Physiol.* **1973**, *51*, 174−187.

(4) Kiefer, L. L.; York, W. S.; Albersheim, P.; Darvill, A. G. Structural characterization of an arabinose-containing heptadecasaccharide enzymically isolated from sycamore extracellular xyloglucan. *Carbohydr. Res.* **1990**, *197*, 139−158.

(5) Kotake, T.; Yamanashi, Y.; Imaizumi, C.; Tsumuraya, Y. Metabolism of l-arabinose in plants. *J. Plant Res.* **2016**, *129*, 781−792.

(6) Krog-Mikkelsen, I.; Hels, O.; Tetens, I.; Holst, J. J.; Andersen, J. R.; Bukhave, K. The effects of l-arabinose on intestinal sucrase activity: dose-response studies in vitro and in humans. *Am. J. Clin. Nutr.* **2011**, *94*, 472−478.

(7) Alton, G.; Hasilik, M.; Niehues, R.; Panneerselvam, K.; Etchison, J. R.; Fana, F.; Freeze, H. H. Direct utilization of mannose for mammalian glycoprotein biosynthesis. *Glycobiology* **1998**, *8*, 285−295.

(8) Freeze, H. H.; Sharma, V. Metabolic manipulation of glycosylation disorders in humans and animal models. *Semin. Cell Dev. Biol.* **2010**, *21*, 655−662.

(9) Rhys, N. H.; Bruni, F.; Imberti, S.; McLain, S. E.; Ricci, M. A. Glucose and Mannose: A link between hydration and sweetness. *J. Phys. Chem. B* **2017**, *121*, 7771−7776.

(10) Powner, M. W.; Sutherland, J. D.; Szostak, J. W. The origins of nucleotides. *Synlett* **2011**, *2011*, 1956−1964.

(11) Banfalvi, G. Why ribose was selected as the sugar component of nucleic acids. *DNA Cell Biol.* **2006**, *25*, 189−196.

(12) Eschenmoser, A. Chemical etiology of nucleic acid structure. *Science* **1999**, *284*, 2118−2124.

(13) Eschenmoser, A.; Dobler, M. Why pentose and not hexose nucleic acids? Part I. Introduction to the problem, conformational analysis of oligonucleotide single strands containing 2′,3′-dideoxyglucopyranosyl building blocks ('Homo-DNA'), and reflections on the conformation of A- and B-DNA. *Helv. Chim. Acta* **1992**, *75*, 218−259.

(14) Otting, G.; Billeter, M.; Wüthrich, K.; Roth, H.-J.; Leumann, C.; Eschenmoser, A. Why pentose- and not hexose-nucleid acids? Part IV. 'Homo-DNA': 1H-, 13C-, 31P-, and 15N-NMR-spectroscopic investigation of ddGlc(A-A-A-A-A-T-T-T-T-T) in aqueous solution. *Helv. Chim. Acta* **1993**, *76*, 2701−2756.

(15) Bielski, R.; Tencer, M. A possible path to the RNA world: enantioselective and diastereoselective purification of ribose. *Origins Life Evol. Biospheres* **2007**, *37*, 167−175.

(16) Springsteen, G.; Joyce, G. F. Selective derivatization and sequestration of ribose from a prebiotic mix. *J. Am. Chem. Soc.* **2004**, *126*, 9578−9583.

(17) Boudaïffa, B.; Cloutier, P.; Hunting, D.; Huels, M. A.; Sanche, L. Resonant formation of DNA strand breaks by low-energy (3 to 20 eV) electrons. *Science* **2000**, *287*, 1658−1660.

(18) Martin, F.; Burrow, P. D.; Cai, Z.; Cloutier, P.; Hunting, D.; Sanche, L. DNA strand breaks induced by 0−4 eV electrons: the role of shape resonances. *Phys. Rev. Lett.* **2004**, *93*, 068101.

(19) Sanche, L. Low energy electron-driven damage in biomolecules. *Eur. Phys. J. D* **2005**, *35*, 367−390.

(20) Ptasińska, S.; Denifl, S.; Gohlke, S.; Scheier, P.; Illenberger, E.; Märk, T. D. Decomposition of thymidine by low-energy electrons: implications for the molecular mechanisms of single-strand breaks in DNA. *Angew. Chem., Int. Ed.* **2006**, *45*, 1893−1896.

DOI: 10.1021/acs.jpca.8b11838
J. Phys. Chem. A XXXX, XXX, XXX−XXX

(21) Im, H.-S.; Bernstein, E. R. On the initial steps in the decomposition of energetic materials from excited electronic states. *J. Chem. Phys.* **2000**, *113*, 7911−7918.
(22) Yin, S.; Bernstein, E. R. Properties of iron sulfide, hydrosulfide, and mixed sulfide/hydrosulfide cluster anions through photoelectron spectroscopy and density functional theory calculations. *J. Chem. Phys.* **2016**, *145*, 154302.
(23) Yuan, B.; Yu, Z.; Bernstein, E. R. Initial mechanisms for the decomposition of electronically excited energetic materials: 1,5′-BT, 5,5′-BT, and AzTT. *J. Chem. Phys.* **2015**, *142*, 124315.
(24) Becke, A. D. Density-functional thermochemistry. III. The role of exact exchange. *J. Chem. Phys.* **1993**, *98*, 5648−5652.
(25) Lee, C.; Yang, W.; Parr, R. G. Development of the Colle-Salvetti correlation-energy formula into a functional of the electron density. *Phys. Rev. B: Condens. Matter Mater. Phys.* **1988**, *37*, 785−789.
(26) Becke, A. D. Density-functional exchange-energy approximation with correct asymptotic behavior. *Phys. Rev. A: At., Mol., Opt. Phys.* **1988**, *38*, 3098−3100.
(27) Frisch, M. J.; Trucks, G. W.; Schlegel, H. B.; Scuseria, G. E.; Robb, M. A.; Cheeseman, J. R.; Scalmani, G.; Barone, V.; Mennucci, B.; Petersson, G. A., et al. *Gaussian 09, Revision A.02*: Gaussian, Inc.: Wallingford, CT, 2009.

DOI: 10.1021/acs.jpca.8b11838
J. Phys. Chem. A XXXX, XXX, XXX−XXX